Abstract

Unmixing Space Object's Moderate Resolution Spectra

Phan Dao, Patrick McNicholl and Anthony Dentamaro
AFRL/RVBYC
Eileen Ryan and William Ryan
New Mexico Tech

Many non-resolved techniques have been proposed and explored to infer space object's characteristics that may lend insight to object's identification and status. The latter attributes are hard to obtain in the absence of resolved imagery, as for objects not in Low Earth Orbit or for small-sized ones. Spectral unmixing is a non-resolved technique that derives an object's material composition from one or a series of spectra. While spectral unmixing techniques have been tested with space objects and spectrometric visible spectra, with spectral width smaller than 0.4 nanometers and over 100 spectral channels, its success against moderately resolved spectra has not been verified. An example of a moderate resolution sensor is that of a slit-less spectrograph which is desirable because of its simple implementation and arguably better temporal fidelity than systems with a slit. A moderate number of spectral bands are considered a challenge when the number of bands is much smaller than the number of material candidate spectra. We develop the Spectral Unmixing for Space Objects (SUSO) algorithm based on Sparse Recovery optimization techniques to deal with this challenge. Sparse recovery, a specialty area of Compressive Sensing, capitalizes on the knowledge that, while the number of candidate materials is expansive, the external surface of a satellite is effectively composed of a few representative materials. We discuss the technique and show the results of applying it on a number of simulated and measured spectra. Simulated signatures are in the Visible and reflective IR, and measured signatures were made with the Magdalena Ridge Observatory's slit-less spectrograph, which is based on a CCD and grating combination mounted on a 2.4 m telescope. We studied the preservation of temporal information when a time series of spectra is analyzed by SUSO and the prospect of augmenting typical shape recovery with material attribution.

Abstract for AMOSTECH 2013
September 2013
Maui, Hawaii, United States

Public Release form:

377th Air Base Wing
Office of Public Affairs
Release #: 377ABW-2013-0719
OPS #: OPS-13-5257

1. INTRODUCTION

Resolved imagery is generally not available for space objects in MEO and GEO because of the large observation range. Even for objects at altitude only a few thousands of km, spatial resolution sufficiently high to determine their status and functionality is not attainable with optical telescopes. Therefore researchers have to develop non-resolved techniques to harvest additional information. For three-axis stabilized geostationary objects, information contained in the temporal domain reveals only rudimentary information about their characteristic albedo-area products and solar panel orientation. It is the goal of this research effort to exploit spectral information and derive more exquisite information needed to identify, characterize and assess a satellite's capability. Spectral unmixing techniques have been reported by the AFRL AMOS group [Luu 2003]. Luu has successfully demonstrated that spectral signatures collected with the SPICA spectrometer, mounted on the 1.6 meter telescope, could be decomposed to infer fractional abundances of candidate materials. Material-based identification and characterization would be possible as a result of spectral unmixing. In the visible, the non-resolved spectral signature is modeled as a linear mixture of spectral reflectance signatures, assumed to exist in an *a priori* library. The mixing coefficients are determined by the viewing aspect. The mixing is justifiably linear because the sun illuminates the object directly, and the source spectrum is the uncorrupted solar spectrum. Such a system can be represented by the following equation.

$$y = aA + noise \qquad (1)$$

with

A=vector of actual abundance coefficients or areas
y=mixed spectral signature
a=matrix of spectral signatures in library

The unmixing algorithm is applied to the mixed signature to determine the coefficients of abundance or apparent areas. For the problem of characterizing space objects, *A* is defined as the apparent area which will be defined and discussed later. The spectral signature *y* is a (n x 1) column vector for the *p* wavelengths or spectral bands. The vector of abundance coefficients has the dimension of (p x 1) for the p candidate materials that exist in the library of spectral reflectance. The dimension of matrix a is (n x p) and each column vector is an unmixed spectral signature for the material. In the hyperspectral unmixing community, the material spectral vector is called an end-member. The simplest solution, in order to find an estimate $\hat{A}$ of A, is to multiply the inverse of matrix a by the observation vector y ($\hat{A} = a^{-1}y$). However, this is not possible because the matrix a is not square, therefore not invertible and we have to deal with an ill-posed problem. When terrestrial hyperspectral data is available, it is typical that $n \gg p$ because the number of candidates (e.g., grass) is small. For space object's spectral unmixing problems, p, the number of material candidates, is typically in the order of several hundred, while n could be in the thousands for a high resolution spectrometer, such as the one used by the authors of [Luu 2003]. In this paper, we investigate a technique that can be used for a moderate number of wavelengths and for $n < p$. The impetus is to lower the requirement of spectral

resolution, improve affordability and make use of a more robust multispectral sensor such a slit-less spectrograph.
While not described in [Luu 2003], the abundance and the known material identity can be used to estimate the apparent area of each present material. The technique used to unmix the signature is characterized as a nonlinear conjugate gradient method of minimizing the Euclidian distance (l_2 norm) between the observed spectrum and the forward model's signature. The objective function to minimize is as follows.

$$\hat{A} = \arg min_A \ \|y - aA\|_2 \qquad (2)$$

where $\hat{A}$ is an estimate of the vector of abundance coefficients. The cost function is the sum of the squares of the differences between the observed y and the forward model's aA. The use of l_2 norm in (2) is typical in a least-squares technique. Without noise, minimization based on (2) provides an exact solution. As discussed in [Luu 2003], constraints of non-negativity and flux conservation are added to the optimization to ensure that the solutions are physically consistent. For the applications envisioned in [Luu 2003], where the number of wavelengths *n* is both large and larger than the number of candidates *p*, this technique works fairly well.

We note that for most satellites, the number of materials with sufficiently significant external surfaces is a small number typically less than 10. As the number of candidates contained in a signature is usually small, the vector of fractional abundances A is sparse and the unmixing process requires solving a combinatorial problem, which demands significant computational efforts. Fortunately, these difficulties can be alleviated by efficient sparse regression techniques which are recently developed for terrestrial hyperspectral problems. [Iordache 2011] recognized that for a noisy signature, the presence of noise and the ill-conditioned nature of a -hence small eigenvalues of its SVD decomposition- lead to a large error in the estimate of *A* and a loss of its sparsity. In order to reduce the effect of the ill-conditioned nature of matrix a, one can encourage a sparser solution by including a sparsity inducing term to the objective function. Of the two possible sparsity enforcing terms, $\|A\|_0$ and $\|A\|_1$, the later has been shown by [Bruckstein 2009] to be effective when the matrices a are "incoherent" and the vectors A are known to be sparse. The discussion of incoherence is beyond the scope of this paper but we propose, and will discuss, the pruning of the spectral library based on pairwise spectral angles as a means to promote incoherence. Candes, Romberg and Tao [Candes 2006] provided the mathematical proof that l_1 can be used instead of l_0 and hence introduced the foundation of Compressive Sensing (CS). It is interesting to note the relationship between sparse spectral unmixing techniques and CS techniques is more fundamental than the mere use of a common mathematical tool. Minimizing the l_0 norm, or the number of non-zero coefficients, achieves exactly what is desired but requires solving a difficult non-convex problem. Following Bruckstein and Bioucas-Dias, we use the following l_1-l_2 optimization instead.

$$\hat{A} = \arg min_A \ \|y - aA\|_2 + \frac{1}{\lambda}\|A\|_1 \qquad (3)$$

In (3), the first term expresses the Euclidian distance (l_2) between the observed data and the forward model. The second term (l_1) describes the lack of sparsity in the solution. The regularization

parameter λ controls the relative weight of the two terms. In this paper, we will demonstrate the utility of our Spectral Unmixing for Space Objects (SUSO) algorithm which is based on the minimization scheme described by (3). As discussed, SUSO is designed to work with non-resolved spectral signatures of moderate resolution: $n \approx 20$. The ability to obtain useful sparse solutions for an underdetermined system of equations depends on two factors. The first factor is the degree of coherence between the column vectors of a. The second factor is the degree of sparseness of the original *A*. SUSO is used with space object's simulated data and data measured with the Magdalena Ridge Observatory's sensor. There was another attempt to apply l_1-l_2 optimization to the unmixing of spacecraft spectrally resolved and spatially resolved imagery reported by Shi et. al. [Shi 2011], but that demonstration was different from ours in two aspects. The spectral signature to unmix is that of a resolved image, and the tests the authors conducted were on simulated data.

2. TECHNIQUES

It is crucial that the spectral library we use is a good representation of material spectral signatures of spacecraft in space. We assume that the effect of ageing on the spectra at GEO is gradual and as long as the study is on relatively new objects with age less than 10 years, the imperfectness of the library can be tolerated. The library is based on that of the Time-domain Analysis Simulation for Advanced Tracking (TASAT) developed and maintained by AFRL. The TASAT 10.0.03 database, file MATTER.DAT (Mat DB Version 5.6) [TASAT 2011], contains optical properties data for 224 types of spacecraft materials and reflectance data for eight Earth topographical surfaces. We down-select to 171 candidate sets with the greatest number of entries being for films and insulators, followed by metals, solar panel materials and paints.

For many materials, spectral reflectance values are listed for λ = 200nm -14μm; more than half of these candidate sets contain more than 300 wavelength entries, and two-thirds provide data for at least 200 spectral values, with visible wavelengths (λ < 1μm) being well-represented in the general case. Although MATTER.DAT presents a comprehensive source of spectral information for different types and alloys of various materials, many entries are not spectrally distinct, and the candidate list of n materials can be pared down rather quickly. Information found in MATTER.DAT can be supplemented by other sources, such as the 2004 NASA JSC Spacecraft Materials Spectral Database [NASA 2004]. The NASA database contains 263 materials, many of them from actual spacecraft surfaces, at 3 nm resolution in the region 0.35 – 2.5 μm. Although there is some redundancy between the materials listed in the NASA database and those in the TASAT file, the former provides reflectance values for many specific spacecraft-type surfaces.

While we have discussed the solutions as abundance coefficients, the pertinent value is the apparent area *A*. The value *A* we can determine with SUSO includes the normalized unit-less reflectance. The spectrally measured flux contains both area information and spectral information. The bidirectional reflectance distribution function (BRDF) is defined as $f_r \equiv \frac{dL}{dE}$,where *L* is the outgoing radiance, *E* the incoming irradiance and the use of differentials is used to keep track of the radiance due solely on a specific illumination in case there are more than one sources. All three quantities in the expression depend on the direction of the sun as well as the direction of the observer. For common materials, f_r is the product of reflectance (albedo) *a* and the angular distribution function shown in (4)

$$f_r \equiv a \cdot f_\theta$$
$$f_\theta \equiv \frac{1}{a} \cdot \frac{dL(\vec{o})}{dE(\vec{s})} \quad (4)$$

where $\vec{o}$ and $\vec{s}$ are the target to observer and target to sun vectors. f_θ is the angular distribution function or normalized BRDF. For a Lambertian material $f_r = \frac{a}{\pi}\cos(\theta_s)\cos(\theta_o)$ and its normalized BRDF $f_\theta = \frac{cos(\theta_s)\cdot cos(\theta_o)}{\pi}$ $[sr^{-1}]$. We'd prefer to write the BRDF f_r as product $a\, f_\theta$ (Eq. 4) to separate the solvable albedo *a* from the angular distribution function. The expression for the in-band flux *F* received by a telescope of aperture *D* from an object of area A_{true} at distance *z* is as in (5)

$$F(\overline{\lambda}) = a(\overline{\lambda}) \cdot f_\theta \cdot A_{true} \cdot T(\overline{\lambda}) \cdot \frac{\pi D^2}{4\, z^2} \int_{\lambda_1}^{\lambda_2} F_{sun}(\lambda) QE(\lambda) d\lambda \quad (5)$$

where F_{sun} is the solar flux, $QE(\lambda)$ is the detector's quantum efficiency and *T* is an all-inclusive efficiency that includes the effects of optics and the atmosphere. Defining the apparent area *A* as

$$A = f_\theta\, A_{true} \quad (6)$$

we can convert the measured flux F to a quantity $y = a\, A$, since all other factors are whether known or can be determined by calibration. In practice, flux and spectral calibrations are achieved with calibration stars; therefore *T* and *QE* can be derived by measurements. Spectral calibration is relatively more stable with respect to time than flux calibration. The latter is sensitive to the presence of thin clouds and aerosols. Some data sets are recorded with compromised total flux calibration and have large uncertainty. The problem is reduced to decomposing the total albedo-area product into albedo-apparent area product for each material. It is important to note that the sum of *y*s is constrained by the total measured flux in SUSO.

Note that A is related to the true geometrical area via the normalized BRDF. In the case of a Lambertian surface, the following relationship holds.

$$A = A_{true} \cos(\theta_o) \cos(\theta_s) \quad (7)$$

For a glinty surface, such as a solar panel material, the derived *A* would overestimate the true area if the sensor measures the glint directly and underestimate it if it misses the reflected light. We will show an example to illustrate the effect.

The spectral angle between two spectral signatures *s (n x 1)*, typically used to compare spectral shapes and classify them, is defined as follows.

$$\alpha = cos^{-1}\left(\frac{s_1 \cdot s_2}{|s_1| \cdot |s_2|}\right) \quad (8)$$

To reduce the dimensionality of the spectral library, whether by eliminating redundancy or grouping signatures with a similar shape, we sort all signatures in separate groups. All members in a given group are required to have less than a threshold angle from a group's representative. When the threshold is chosen to be 2 degrees, the visible MATTER.DAT library can be pruned to a library with only 35 distinct materials. The library's size increases to 57 when the threshold is 4 degrees.

3. SPECTRAL MEASUREMENTS

The instrument setup utilizes the Magdalena Ridge Observatory (MRO) 2.4-meter telescope and consists of a blazed 100 line/mm transmission grating mounted in the facility filter wheel for easy accessibility. This places the grating in an f/8.9 converging beam approximately 195 mm in front of the focal plane. The resulting first order spectra have a dispersion of 56.2 nm/micron with a length of ~7 mm over the wavelength range 400 to 800 nm. The spectra are imaged using an Andor iKon 936 CCD camera with a 2Kx2K EEV CCD42-40 array and 13.5 micron pixels thermoelectrically cooled to -85^{o}C. Typical realized seeing is on the order of one arc-sec, and the CCD is binned 4x4 resulting in approximately 2 pixels or 6 nm per seeing width. Hence, a 20 nm spectral bin will be sufficiently sampled even in poorer seeing conditions.

The raw data product is a two-dimensional FITS image as shown in Figure ~~X~~1 below. The images are bias- and dark current- subtracted to remove the background. Since the current grating also introduces some vignetting, flat fields are acquired, and then the large scale gradients are removed before applying them to the object images. This has the effect of correcting for pixel to pixel variations while leaving the large scale gradients untouched, given that trying to separate these spatial gradients from color sensitivities is a dubious procedure at best. For GEO satellites, the zero order image is placed near the edge of the un-vignetted field which allows the full first order spectra to still be captured on the chip. When possible, we try to place any calibrations stars at the same position in an attempt to minimize effects of any large scale gradients ignored in the flat-fielding process are canceled out. For the current work, five images were taken and then realigned before median combining to help ensure that the effect of any interloping star trails was removed.

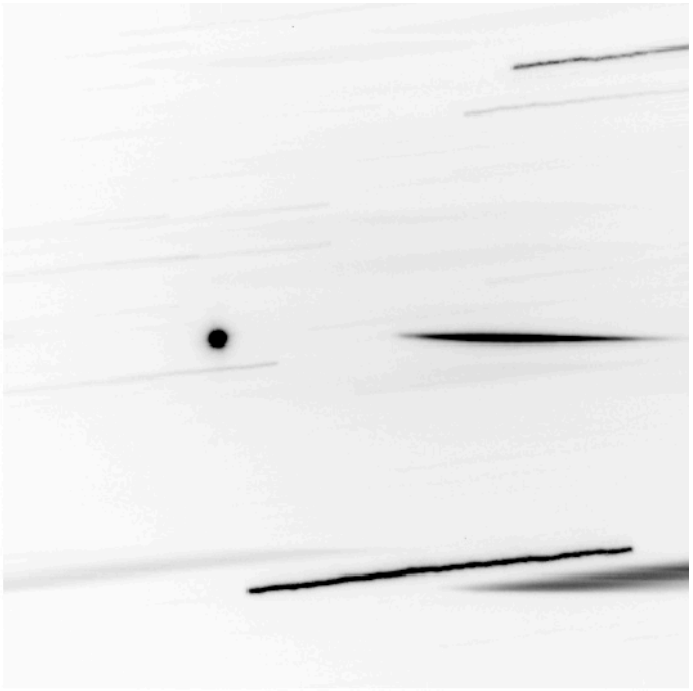

Figure 1. Raw image of a single 10 sec exposure of VENESAT-1 (33414) which includes the zero- and first-order images captured horizontally along the center. Contaminating field stars (angled streaks in the above image) are eliminated by median combining five raw.

One dimensional spectra are extracted by defining three strips along the dispersion axis – one containing the spectra and two on each side containing a local background. For this analysis, the IRAF tasks *twodspec* and *onedspec* were used for the extraction and later, the calibration. However, both MATLAB and IDL-based software are under development to identify the most productive pipeline processing system. More precise spectral dispersion is determined by acquiring spectra from a number of Wolf-Rayet stars and fitting the positions of the prominent emission lines. The data are then divided into 20 nm segments and each bin is summed resulting in a spectrum as shown in Figure 2~~1~~.

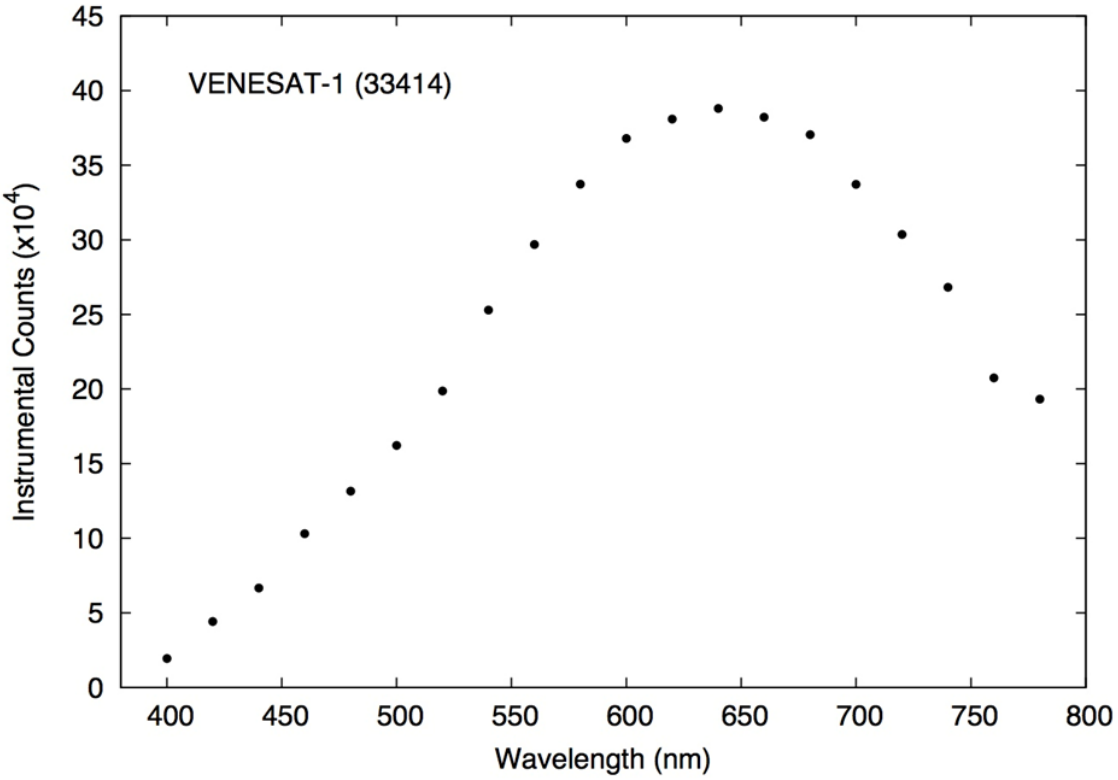

Figure 2. Summed spectra (in 20 nm bins) extracted from the median of five of the single images shown in Figure 1.

The spectra are then flux-calibrated by observing standard stars with known spectrophotometric flux calibrations [Oke 1990] at similar air masses as the target objects. Analyzing these spectra permits the determination of the calibration function due to the instrument sensitivity and atmospheric transmission, which is then applied to the target objects resulting in spectra having the units ergs/cm^2/s. Analysis of other spectrophotometric stars used as check objects indicates that this procedure results in calibrations good to a few percent.

4. RESULTS

The following results illustrate the nature of the apparent areas retrieved by SUSO. MRO observed VENESAT-1 on two occasions: February 7 and June 21, 2013. The two line element set of

VENESAT-1 was obtained in the public domain as listed as its COSPAR designation 2008-055A. Near equinox, the geometry of the view from MRO is such that the glint dominates the signature. Figure 3 shows a waterfall display of the reflectance spectra measured in February.

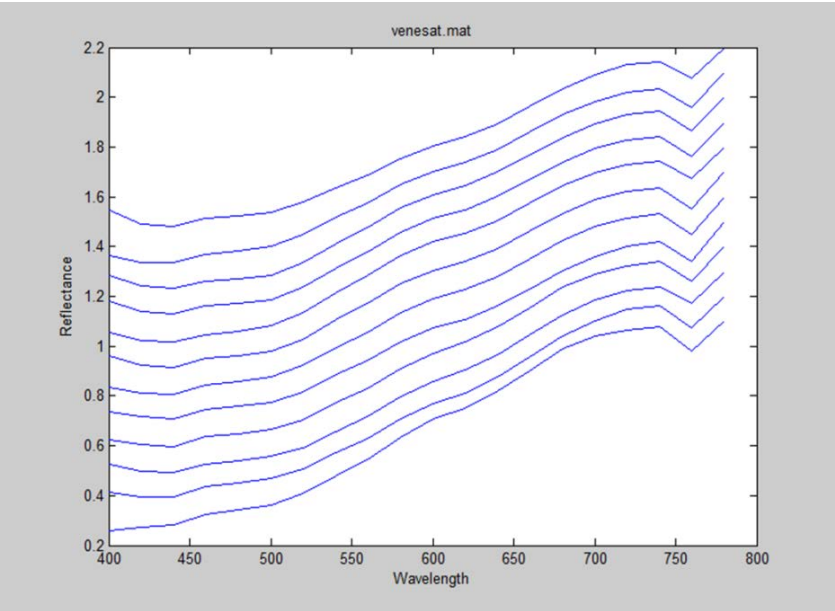

Figure 3. Spectra measured by MRO on February 5, 2013.

The plot of material identification is shown in Figure 4. The list of retrieved materials are as follows.

ID	Area	MATTER.DAT description		
material 7	0.54	SURF	0011	Copper
material 8	0.82	SURF	0012	Beryllium Copper Alloy
material 12	0.88	SURF	0026	Kapton, Aluminized, 1 Mil,Kapton
material 18	2.96	SURF	0075	Phenolic Block, Linen Filled
material 34	1.27	SURF	0237	GaAs ATJ Solar Array #1,Emcore,Max

The retrieval by SUSO identified the solar panel to be based on GaAs solar cells. It is worth noticing that the presence of the glint in the spectral signature allows the identification of the solar panel material. By contrast, for the series of spectral signatures collected on June 21, the condition of reflection is not met and, no material associated with the solar panel is retrieved. The materials retrieved in the June 21 spectra are as follows

material 7	0.63	SURF 0011 Copper
material 12	0.58	SURF 0026 Kapton,Aluminized,1 Mil,Kapton side out
material 16	0.86	SURF 0072 Aluminum Alloy,7075-T6,Alodined
material 18	1.08	SURF 0075 Phenolic Block,Linen Filled

We showed this example to demonstrate that the apparent area of the solar panel derived by SUSO depends of the illumination and viewing conditions. At solstice, the solar glint from the panel is not recorded by the sensor because of unfavorable conditions and no material identified with the solar panel can be retrieved. The quantity that can be retrieved, while proportional to the true area, is mitigated by the BRDF of the surface. For this satellite, the solar panel is expected to be stabilized with respect to the sun. The most likely attitude is for the solar panel to pivot about a polar axis, such that the normal to the panel and the sun vector are coplanar. Under those conditions, the glint at solstice will be ~20 deg north of MRO, and it is expected that the spectral signature does not have a contribution from the solar panel. In general, materials retrieved by SUSO for VENESAT-1 and other satellites correspond to typical spacecraft materials. We have not begun to validate the results except to notice that the results have been plausible given the types of satellites we have observed and retrieved.

5. DISCUSSIONS AND CONCLUSIONS

We have begun to analyze the results of retrieving material identities from spectral signatures collected by MRO. The results are considered to be preliminary and too premature for validation. While an effort to validate the technique with simulation has been conducted, we do not include the results in this report. The ultimate objective of this research is to build an algorithm that attributes material to individual facets with known orientations. Knowledge of orientation will remove the ambiguity in material's area because the angles needed to estimate the BRDF factor in (6) would be known. Since the information needed to retrieve facet's information is encoded in the temporal evolution of the material composition, we want SUSO not to introduce spurious noise and corrupt temporal fidelity. We discovered in our tests of simulated spectral signatures for which the change in material composition is known, that including a total variance (TV) term to the objective help SUSO maintain a higher fidelity temporal signature. The TV term ensures that the composition doesn't vary significantly from one spectrum to the next, not by "low pass filtering" the results but by adding a time variation term to the objective (right-hand side of Eq. 3). We have not seen evidence that the use of TV dampened material composition change near a glint. The change of material composition in time is shown in Fig.4 and 5 by the false color of each material. For example, the solar panel material peaks at 5:15 UT while the phenolic block material peaks at 6:18 UT during the February 5, 2013 session.

6. ACKNOWLEDGEMENTS

Support from the Space Object Surveillance Technology Program Manager, Dr. Jeremy Murray-Krezan, and the SSA community at the Space Vehicles Directorate is well appreciated.

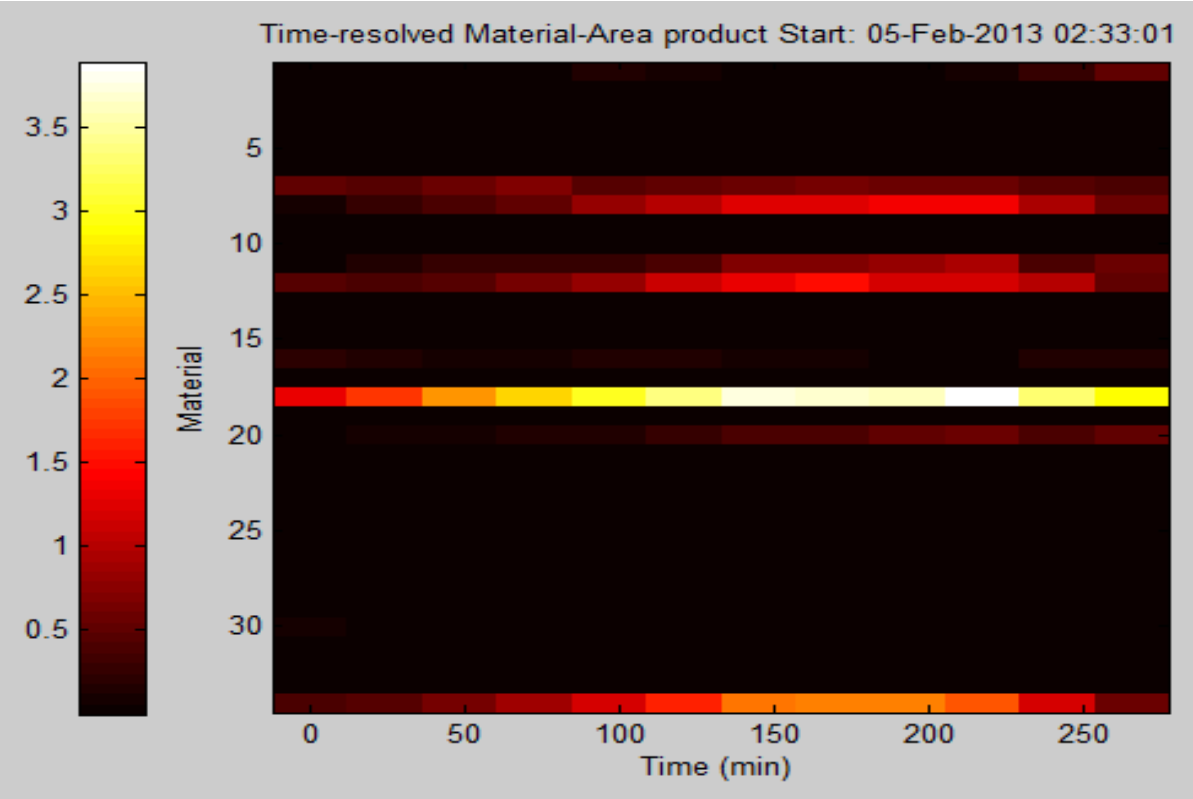

Figure 3. Material decomposition of spectra measured at equinox.

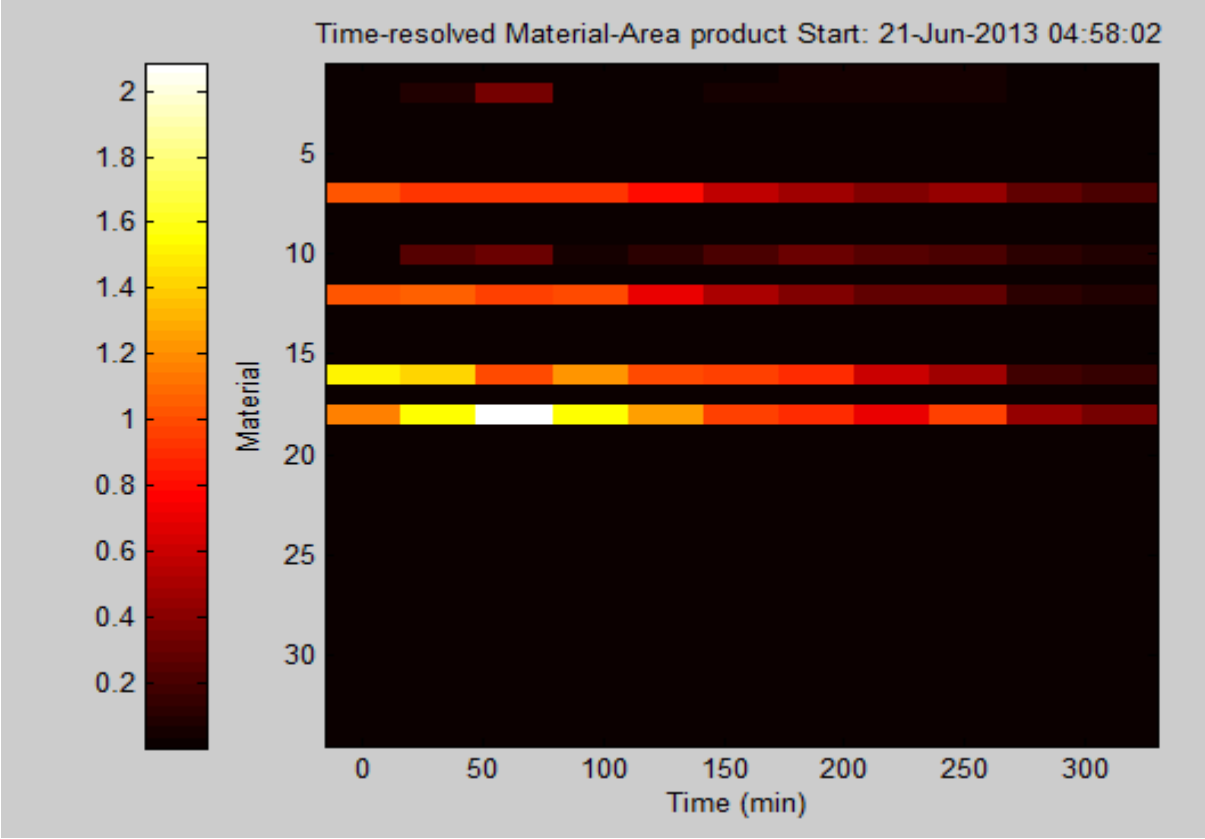

Figure 4. Material decomposition of spectra measured at solstice.

References

[Luu 2003] K. Luu, C. Matson, M. Giffin, K. Hamada, J. Lambert, and J. Snodgrass, Object Characterization from Spectral Data, 2003 AMOS Technical Conference, Maui, Hawaii, 8-13 September 2003.

[Bruckstein 2009] A. M. Bruckstein, D. L. Donoho, M. Elad, *From Sparse Solutions of Systems of Equations to Sparse Modeling of Signals and Images*, SIAM Review, vol. 51, no. 1, pp. 34-81, 2009.

[Candes 2006] E. Candès, J. Romberg, and T. Tao, "Stable signal recovery from incomplete and inaccurate measurements," Commun. Pure Appl. Math., vol. 59, no. 8, pp. 1207–1223, Aug. 2006.

[Shi 2011] Zhenwei Shi, Xinya Zhai, Durengjan Borjigen and Zhiguo Jiang, *Sparse unmixing analysis for hyperspectral imagery of space objects*, Proc. SPIE 8196, International Symposium on Photoelectronic Detection and Imaging 2011: Space Exploration Technologies and Applications, 81960Y, August 15, 2011.

[TASAT 2011] TASAT 10.0.03 database, file MATTER.DAT (Mat DB Version 5.6), Satellite Assessment Center (SatAC), AFRL/RD, Kirtland AFB, NM 87117, 2011.

[NASA JSC SMSD 2004] NASA JSC Spacecraft Materials Spectral Database, NASA JSC, 2004.
[Oke 1990] Oke, J. B. 1990 Faint Spectrophotometric Standard Stars. Astronomical Journal 99, p1621-1631.